

Studies on the cycle life of commercial lithium ion batteries during rapid charge–discharge cycling

J. Li^{*}, E. Murphy, J. Winnick, P.A. Kohl

School of Chemical Engineering, Georgia Institute of Technology, Atlanta, GA 30332-0100, USA

Received 16 April 2001; accepted 15 May 2001

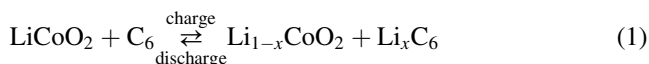
Abstract

The impedance spectra of Li-ion batteries as a function of the number of charge–discharge cycles have been measured to study the cycle life of the commercial Li-ion battery (prismatic Sanyo UF653467) during cycling at 1 C charge–discharge rate. The individual electrodes in the batteries have been examined using XRD, transmission electron microscopy (TEM) and SEM. The results show that the Nyquist plots of commercial lithium-ion batteries are comprised of an inductive tail at high frequency followed by two semicircles at medium and low frequencies. The size of the semicircles at low frequency increase during cycling due to the increase in interfacial resistances of both cathode and anode. Thus, it may be used to predict the cycle life of the battery. XRD, TEM and SEM studies of the individual electrodes show that the cation disorder, microcracks of the LiCoO₂ particles in the cathode and the increase in thickness of the passive film on the anode due to the reduction of the electrolyte are linked to the capacity fade of the battery during cycling. © 2001 Elsevier Science B.V. All rights reserved.

Keywords: Lithium-ion batteries; Capacity fade; Impedance spectrum; Rapidly cycling

1. Introduction

Numerous electrode materials have been developed since the first commercial lithium-ion battery introduced in 1990 [1,2]. Commercial lithium-ion batteries often employ layered LiCoO₂ as the cathode material and graphitized carbon as the anode material because of high working voltage and cell stability [3]. During the charge and discharge process, the lithium ions are reversibly deintercalated and intercalated between the cathode and the anode through a non-aqueous electrolyte, which can be represented as [4]:



In the fully charged state, the potential of the cathode is 4.1 V and the lithiated graphite is nearly 0 V with respect to lithium metal. The cathode material in this state has the composition Li_{0.5}CoO₂ and retains the same layered structure as LiCoO₂ [5]. Thus the lithium-ion batteries with this configuration should retain high capacity except when the

irreversible structural and morphological changes take place in the electrode materials.

However, the capacity retention and lifetime of the lithium-ion battery depend on the structural stability of electrode materials, the electrochemical behavior of the electrodes and internal structural stability of the battery. They involve Li⁺ diffusion within the electrolyte and electrode, ohmic drop, electrolyte decomposition, and interfacial properties between the electrode and electrolyte [6]. Thus, the battery will lose capacity gradually during cycling even under normal operating conditions [7]. At higher charge–discharge rates, the capacity degradation is accelerated.

Impedance spectroscopy is a nondestructive technique and can be used to provide important electrochemical parameters of the sealed battery, such as charge transfer resistance and double layer capacitance, which are useful to evaluate the battery performances [5,8]. For example, Rodrigues et al. were able to predict the state-of-charge (SOC) of the lithium-ion battery by impedance measurements [9]. In this study, we conducted impedance measurements on sealed commercial lithium-ion batteries cycled at 1 C charge–discharge rate to study the cycle life of the battery. Combining with XRD, TEM and SEM techniques, the capacity fading process of commercial lithium-ion batteries during rapid (1 C) charge–discharge cycling were investigated.

^{*} Corresponding author. Tel.: +1-404-894-2893; fax: +1-404-894-2866. E-mail address: paul.kohl@che.gatech.edu (J. Li).

2. Experimental

The lithium-ion batteries used in this study were prismatic Sanyo UF653467 with nominal capacity of 930 mAh. The charge–discharge cycles were performed in pulse protocol under the following regime [10], the battery was charged at 1 C average to 4.1 V, kept for 0.5 h at the open-circuit, and then discharged at the same rate down to 3.0 V. Impedance measurements of the lithium-ion batteries at fully discharged state were carried out by a potentiostat (EG&G PARC model 273 A), equipped with a lock-in amplifier (EG&G PARC model 521 C) and controlled by impedance software Model 398. The amplitude of the alternating current signal was 5 mV over the frequency range between 65 kHz and 25 mHz. The cathodes were used as working electrode and the anode as both the counter and reference electrodes. All measurements were conducted at room temperature.

After that, the discharged batteries were carefully disassembled in an dry box. Both cathodes and anodes were immediately placed into a diethyl carbonate solution (DEC, 99+%, Aldrich) for 5 h to remove the lithium salts adsorbed on the electrodes. The treated electrodes were dried in an inert atmosphere and prepared for microscopy examination. The structural changes of the electrode materials were investigated with X-ray diffraction (Cu K α radiation and graphite filter at 45 kV and 40 mA), and the surface morphologies were observed by means of a scanning electron microscopy (SEM, Hitachi S-800). The internal defects of LiCoO₂ particles were observed using transmission electron microscopy (TEM, JEM 100 C, operating at 100 kV accelerating voltage). Cathode films need to be thinned by sputtering before TEM observation.

3. Results and discussion

3.1. Cycle life of the batteries

The discharge capacity of the lithium-ion battery as a function of the number of cycles is shown in Fig. 1. At the

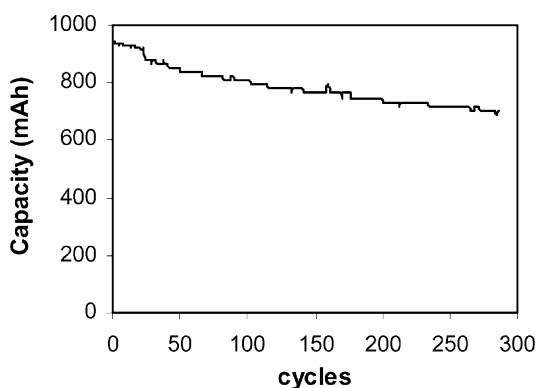


Fig. 1. Cycling performance of lithium-ion battery between 3.0 and 4.1 V at 1 C rate.

Table 1
Discharge capacities of the lithium-ion batteries with different cycle number

	Cycle number		
	0	40	286
Discharge capacity (mAh)	1005	972	703

1 C charge–discharge rate, the discharge capacity of the lithium-ion battery quickly drops. After 286 cycles, the capacity of the battery drops from 1005 to 700 mAh and the loss of capacity is not recovered even at a lower charge–discharge rate. These results indicate some battery components, especially the interfaces between the solid-electrodes and the non-aqueous electrolyte, are changed during cycling. In order to elucidate these changes, the impedance spectra of three lithium-ion batteries at different cycles were measured. The discharge capacities of the batteries are listed in Table 1.

3.2. Impedance studies

The impedance spectrum of the sealed lithium-ion battery reflects the electrochemical processes at the interfaces of both the anode and the cathode. Therefore, the impedance parameters, such as charge transfer resistance and double layer capacitance, involve the interface properties between anode, cathode and electrolyte. Fig. 2 shows the Nyquist plots of the lithium-ion batteries in the completely discharged state as a function of cycle number. As described by other researchers [9,11], the Nyquist plot of a lithium-ion battery is mainly comprised of an inductive tail at high frequency followed by two semicircles at the medium and low frequencies. It can be seen that the size of the low frequency semicircle increases with the number of cycles. Furthermore, there is a very small linear spike following the low frequency semicircle in the impedance spectrum of the new battery, which gradually disappears with increasing cycles. The medium frequency semicircle is depressed and has no distinctive change with increasing cycles. Hence, analyzing impedance parameters, especially the parameters related to the semicircle at low frequency, is useful for prediction of the cycle life of a sealed battery.

Rodrigues [9] evaluated the impedance parameters of the lithium-ion battery at different SOC using the equivalent circuit shown in Fig. 3 and non-linear least squares (NLLS) fitting procedure. We have adopted the same equivalent circuit and procedure to analyze the impedance parameters. Since the small linear spike following the low frequency semicircle did not appear in the Rodrigues' impedance spectra, we here neglect this small feature. In Fig. 3, L is the inductance taken in parallel to a resistance R_L corresponding to the high frequency inductive tail in impedance spectra; R_Ω represents the ohmic resistance of the battery; Q_1 and Q_2 are constant phase elements (CPE), which are taken

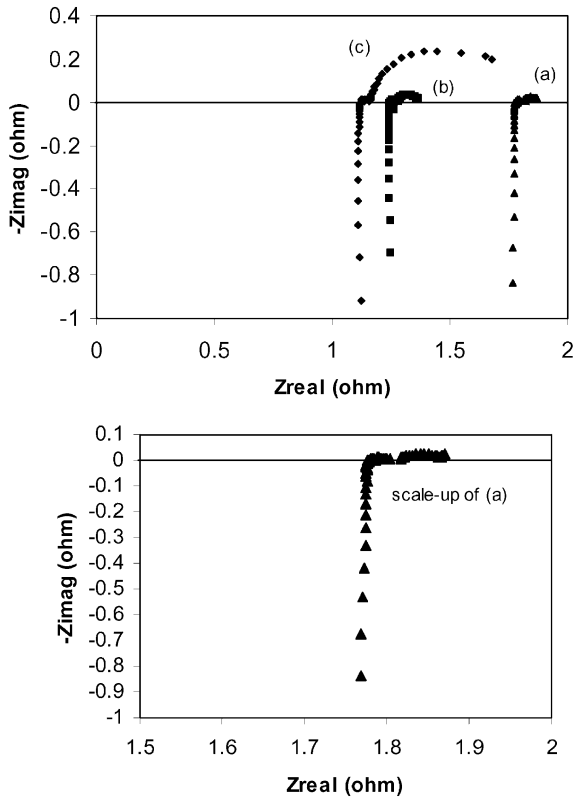


Fig. 2. Impedance spectra of fully discharged lithium-ion batteries with different cycle number at 1 C rate: (a) 0; (b) 40; (c) 286 cycles.

in parallel to the respective resistance R_1 and R_2 corresponding to the medium and low frequency semicircles, respectively [9]. The CPE is a very general diffusion-related element and arises from the fractal nature of the interface between electrolyte and electrode. The CPE is suitable for the lithium-ion battery because the electrodes in the lithium-ion battery are made from fine particles of the active materials and thus the electrodes are neither smooth nor uniform. The admittance representation of the CPE is given by [12]:

$$Y^*(\omega) = Y_0(j\omega)^n = Y_0\omega^n \cos\left(\frac{n\pi}{2}\right) + jY_0\omega^n \sin\left(\frac{n\pi}{2}\right) \quad (2)$$

where Y_0 is the adjustable parameter containing the diffusion coefficient and other parameters which depend on the characteristics of the electrochemical system. For $n = 0$ it represents a resistance with $R = Y_0^{-1}$, for $n = 1$ a capacitance with $C = Y_0$, for $n = 0.5$ a Warburg impedance and for $n = -1$ an inductance with $L = Y_0^{-1}$.

The impedance spectra parameters obtained via NLLS-fit analysis are listed in Table 2. Generally, the inductance

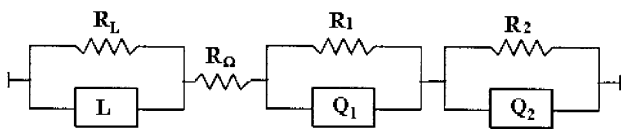


Fig. 3. Equivalent circuit used for NLLS fitting of the impedance spectra of the lithium-ion batteries.

Table 2

Impedance parameters from the lithium-ion batteries with different cycle number

	Cycle number		
	0	40	286
Voltage (V)	3.66	3.71	3.68
R_L (Ω)	91.275	54.461	119.265
L (μH)	2.057	2.017	2.227
R_Ω (Ω)	1.776	1.244	1.121
R_1 (Ω)	0.036	0.032	0.043
Q_1 (Ω^{-1})	2.717	2.226	2.984
n_1	0.461	0.632	0.484
R_2 (Ω)	0.061	0.087	0.505
Q_2 (Ω^{-1})	5.712	5.496	5.187
n_2	0.935	0.901	0.951

behavior of the lithium-ion battery is attributed to the porous features of the electrodes [13,14]. Hence, the value of the inductance L should remain constant during cycling unless the electrodes were mechanically damaged. In addition, the parallel resistance R_L of the inductance does not represent any practical physical process and is only a schematic element for the convenience of the fitting procedure [9]. This is supposed by the random nature of the values for the parallel resistance R_L in Table 2. That is to say, the inductance data is irrelevant in evaluating the cycle life of the battery and analyzing other parameters of the impedance spectrum. R_Ω is the ohmic resistance of the battery, which normally includes the resistance of the electrolyte, current collectors, battery terminals, etc. With increasing number of cycles, it can be seen that R_Ω decreases slightly and the magnitude of the decrease during initial cycling is larger than that during subsequent cycling. Under the normal charge–discharge conditions, the change in ohmic resistance comes mainly from the electrolyte. One possible cause is the formation of the passive films on the surface of the electrodes during initial cycling. This consumes components in the electrolyte, which causes an increase in the concentration of Li^+ in the electrolyte and improves the conductivity of the electrolyte. Since the passive film formation reaction is not reversible, R_Ω tends to be smaller with the increased cycle number.

Although extensive efforts were made in recent years, it is impossible to determine which semicircle in the impedance spectrum corresponds to each electrode (anode and cathode) in the battery because both electrodes contribute to the battery impedance and the kinetics of both electrode reactions are similar in magnitude [8,9]. However, from previous research it may be concluded that the medium-frequency semicircle in the impedance spectrum arises from the passive film on the electrodes, especially on the cathode [9,15]. Thomas et al. [15] suggested that the formation of a passive film on the cathode surface is responsible for the medium frequency smaller semicircle, and R_1 is the resistance of the passive film on the cathode. The formation of the passive film on the cathode is caused by the high potential between

the cathode and the electrolyte interface at the fully charged state. During cycling, this potential causes the electrolyte decomposition on the cathode. The fact that the value of R_1 remains constant and small during cycling indicates that the thickness of the passive film on the cathode remains constant. The change in the constant phase element Q_1 is also not evident. The value of the coefficient n_1 corresponding to Q_1 is close to 0.5, thus Q_1 closely resembles a Warburg impedance.

Since both the anode and the cathode contribute to the semicircle at low frequency, R_2 should be the sum of the interfacial resistances from both the cathode and the anode including the surface film resistances and internal charge transfer resistances. An increase in R_2 is observed during cycling corresponding to the increasing size of the semicircle at low frequency. Hence R_2 is useful in predicting the cycle life of the battery. The value of the coefficient n_2 corresponding to the constant phase element Q_2 is close to 1. Therefore, Q_2 should be capacitive in nature, which slightly decreases during cycling.

3.3. XRD and TEM measurements

X-ray diffraction patterns of the cathode materials at the discharged state with different cycle number are given in Fig. 4. From the characteristic peaks, it can be concluded that the cathode active material is LiCoO_2 , which was confirmed by surface elemental analysis. During cycling, the characteristic peaks of the LiCoO_2 remain the same, thus no new phase is produced. However, the relative intensities of the peaks changed, indicating a change in the structure of the LiCoO_2 phase. Table 3 lists the relative peak intensity ratio between (0 0 3) and (1 0 1) planes. It can be seen that the relative intensity of the main peak (0 0 3) decreases with the increase in cycle number. In the LiCoO_2 phase, alternate layers of Li and Co cations occupy the octahedral sites of a compact cubic close packing of oxide anions. The (0 0 3)

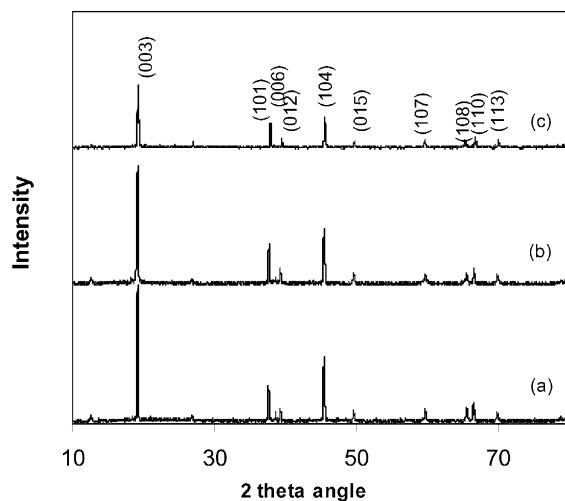
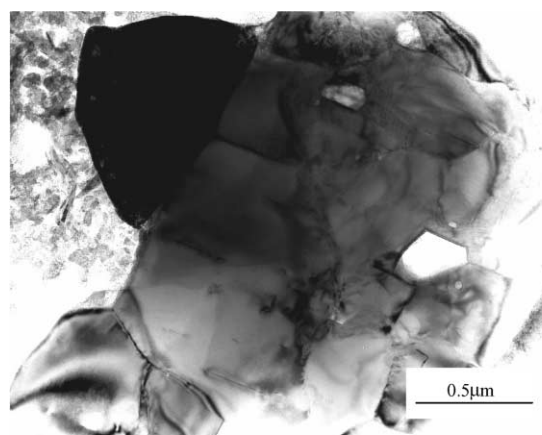


Fig. 4. XRD patterns for cathode materials cycled at 1 C rate: (a) 0; (b) 40; (c) 286 cycles.

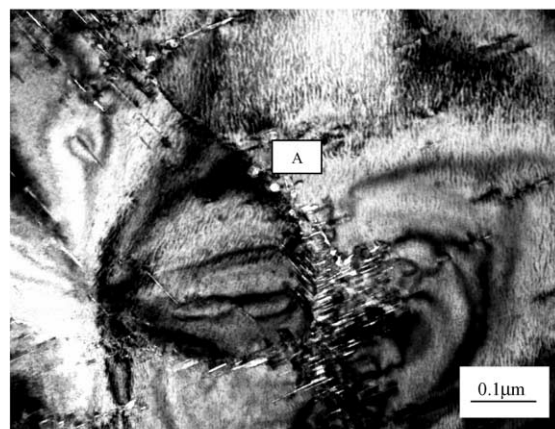
Table 3
Relative change in intensity ratio between (0 0 3) and (1 0 1) plane of LiCoO_2 cathode active materials

	Cycle number		
	0	40	286
Intensity of (0 0 3) plane $I(0\ 0\ 3)$	1556.22	1132.95	687.30
Intensity of (1 0 1) plane $I(1\ 0\ 1)$	452.42	449.30	311.57
$I(0\ 0\ 3)/I(1\ 0\ 1)$	3.44	2.52	2.21

peak intensity decrease would occur when a cobalt atom occupies part of the octahedral sites of the lithium layer [16,17]. Hence, the decrease in the intensity of the (0 0 3) peak during cycling indicates that the cation in the well-layered LiCoO_2 becomes disordered and a portion of the lithium ions in the cathode becomes inactive. The cation disorder in LiCoO_2 can be clearly seen using electron diffraction and is suggested to come from the strain caused by the volume change induced by the intercalation–deintercalation of lithium ion during cycling [18]. The



(a)



(b)

Fig. 5. TEM bright-field images of the LiCoO_2 particles cycled at 1 C rate: (a) 0; (b) 286 cycles.

bright-field images of the LiCoO_2 particles in a new battery and in the battery cycled through 286 cycles are shown in Fig. 5. Compared with the LiCoO_2 particle in a new battery, numerous cracks and pores (A point in Fig. 5(b)) appear in the LiCoO_2 particle after 286 cycles. These cracks and pores can cut off the diffusion channels of Li^+ ion during cycling and decrease the utilization of the active material. In addition, the partial decomposition of LiCoO_2 resulting from the high potential when the battery are in the fully charged state [19] and the passive film formation on the cathode could also contribute to the capacity decrease of the cathode.

X-ray diffraction patterns of the anode materials are shown in Fig. 6. It is clear that the anode is graphitized carbon because of the strong (0 0 2) peak. From the flat potential plateau in the discharge profile of the battery, the anode active material should be graphite. Both the intensities and positions of the characteristic peaks of the graphite electrode do not change during cycling.

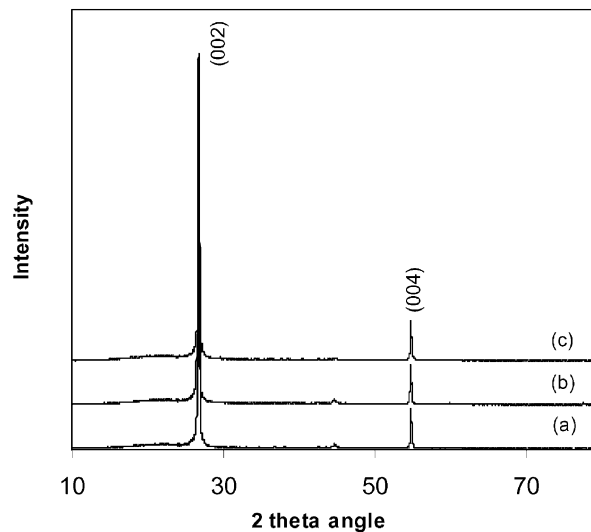
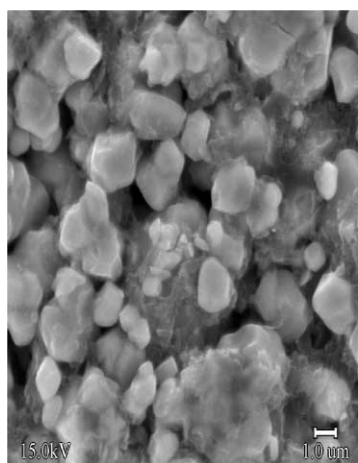
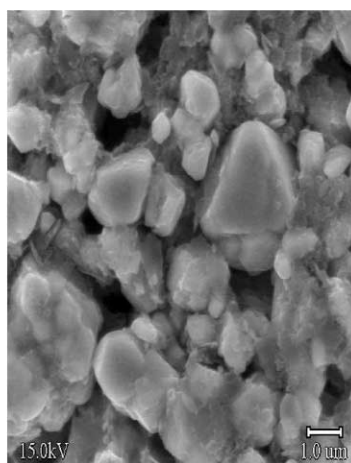


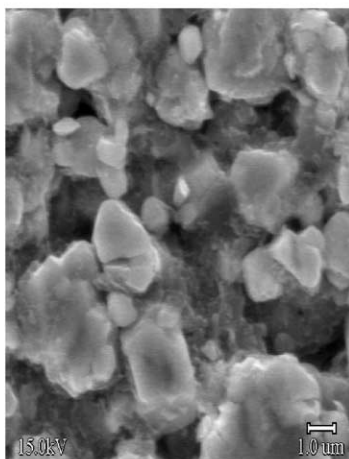
Fig. 6. XRD patterns for anode materials cycled at 1 C rate: (a) 0; (b) 40; (c) 286 cycles.



(a)



(b)



(c)

Fig. 7. Micrographs of cathodes in the fully discharged lithium-ion batteries with different cycle number at 1 C rate: (a) 0; (b) 40; (c) 286 cycles.

amorphous peak at about $2\theta = 20^\circ$ in the graphite electrode is also unchanged, which indicates the stable graphitization of the anode active material during cycling.

3.4. SEM observation

The surface morphologies of the cathodes are shown in Fig. 7. It can be seen that the active material on the current collector stays compact. The average size of the LiCoO_2 particles is about $1\ \mu\text{m}$ and one layer of conductive additives uniformly wraps the active particles. The surface of the cathode experiences no apparent change during cycling, which is in agreement with the stable R_1 in impedance analysis. However, gaps are observed on some LiCoO_2 particles after 286 cycles. A relation to the XRD and TEM results, this is maybe due to the strain induced by volume change during cycling.

The anode active material consists of larger particles than those seen comprising the cathode and some changes were observed on the surface of the anode with increasing number of cycles. As shown in Fig. 8(c), many deep cracks appeared on the surface of anode after 286 cycles and a layer of passive film with a detectable thickness can be observed by naked eye. After removing the passive layer, the surface morphology of the anode presented in Fig. 8(d) is similar to that of the anode in a new battery. Hence, the cracks on the anode surface did not arise from the graphite particles themselves but from the passive film on the anode. The passive film covers the surface of the anode and continuously increases in thickness during cycling. After drying, the thick passive film will break because of higher stress. The formation and increasing thickness of the passive film on the anode is due to the continuous reduction of organic components in the electrolyte during cycling [20,21].

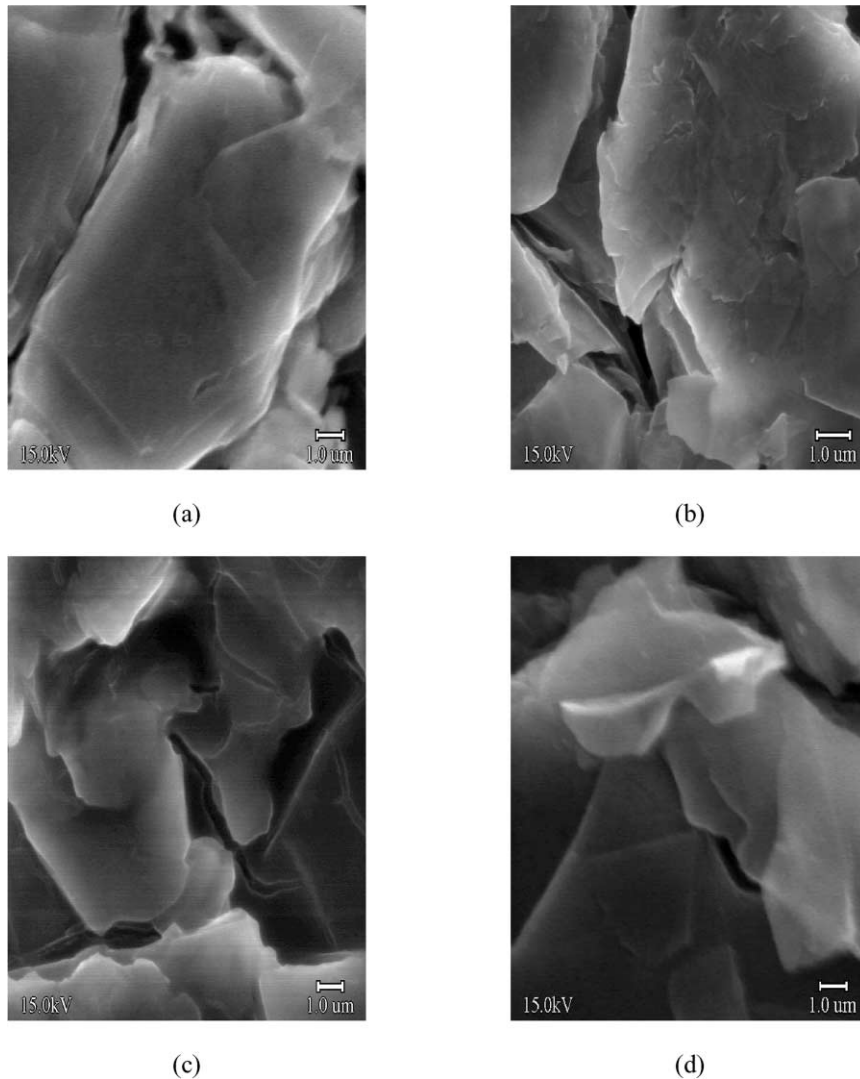


Fig. 8. Micrographs of anodes in the fully discharged lithium-ion batteries with different cycle number at 1 C rate: (a) 0; (b) 40; (c) 286; (d) 286 cycles after removing passive film.

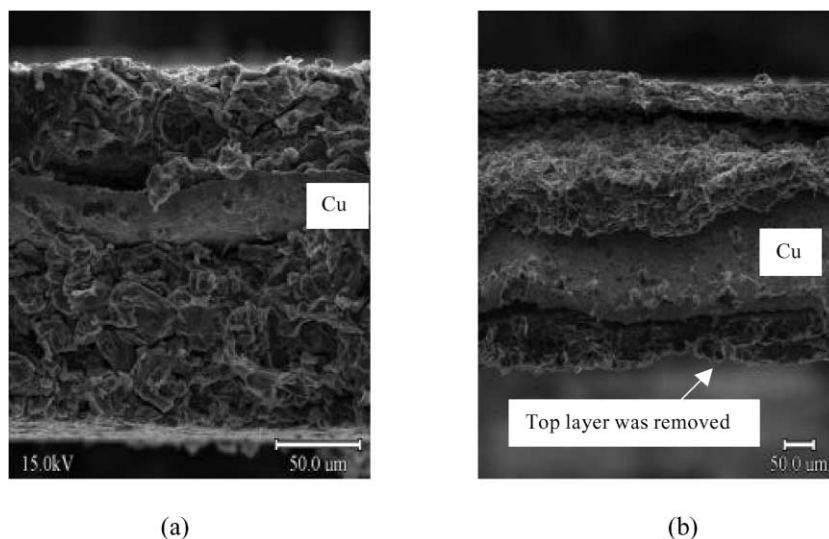


Fig. 9. Micrographs of the cross-sections of anodes in the fully discharged lithium-ion batteries with different cycle number at 1 C rate: (a) 0; (b) 286 cycles.

Fig. 9 show the cross-sections of the anode after 286 cycle and the anode in a new battery. Obviously, the graphite anode on the copper current collector is separated into two layers after 286 cycles. EDS analysis indicated that the top layer which contacts the electrolyte contains more P and F elements than the layer which contacts the copper collector. It is easily to understood that the penetration of the electrolyte species into the anode and the passive film thickness increase make the mechanical properties of the top layer of the anode be different from the inner layer, and thus make the anode be separated at the dry condition.

The thicker passive film can function as a shield that effectively hinders the Li^+ ions from penetrating through to the active electrode [22], thus contributes to the increase in the interfacial resistance of the anode. On the other hand, the process of passive film increase itself must also cause capacity fade because of the consumption of the electrolyte components. It is not clear how the increase of the passive film on the carbon electrode influences the capacity drop, despite the many investigations of the irreversible capacity loss in the carbon anode due to the formation of a solid-electrolytic interface in the initial charge–discharge cycle [23].

In addition, it is worthy to note which electrode contributes more to the capacity fade of the battery, cathode or anode. Up to now, the processes that are known to lead to capacity fade in lithium-ion batteries include lithium deposition (over-charge condition), electrolyte decomposition, active material dissolution, phase changes in the electrode material, and passive film formation on the electrode and current collector surfaces [24]. Some researchers monitored the individual electrode charge–discharge behaviors and measured the interfacial resistances of the electrodes by inserting a reference electrode into the battery during cycling [6,7,11]. The conclusions from all of them are that the cathode determines the discharge capacity of lithium-ion

battery and dominates the total interfacial resistance of the battery.

4. Conclusion

The capacity of the commercial Li-ion battery (prismatic Sanyo UF653467) rapidly fades during cycling at 1 C charge–discharge rates. After 286 cycles, the capacity of the battery dropped from 1005 to 700 mAh. The impedance measurements of the batteries show that the Nyquist plot of the commercial lithium-ion battery is comprised of an inductive tail at high frequency followed by two semicircles at medium and low frequencies. The size of the semicircles at low frequency continuously increases during cycling, which indicates the increasing interfacial resistances of both the cathode and the anode. Thus, it can be used to predict the cycle life of the battery. Studies of XRD, TEM and SEM on the individual electrodes indicate that the formation of the defects such as cation disorder and cracks in cathode active material LiCoO_2 and the continuous increase in the passive film thickness on the anode due to the reduction of the electrolyte are correlated with the capacity fade of the battery during cycling.

Acknowledgements

The enrev Corporation provided partial funding for this work.

References

- [1] A. Rougier, P. Graveau, C. Delama, J. Electrochem. Soc. 146 (1999) 1168.

- [2] R.J. Gummow, A. De Kock, M.M. Thackeray, *Solid State Ion.* 69 (1994) 59.
- [3] M. Broussely, P. Biensan, B. Simon, *Electrochim. Acta* 45 (1999) 3–22.
- [4] R. Alcantara, P. Lavela, J.L. Tirado, E. Zhecheva, R. Stoyanova, *J. Solid State Electrochem.* 3 (1999) 121–134.
- [5] V. Ganesh Kumar, N. Munichandraiah, A.K. Shukla, *J. Appl. Electrochem.* 27 (1997) 43–49.
- [6] W. Wu, W. Lu, J. Prakash, *J. Power Sources* 88 (2000) 237–242.
- [7] D. Zhang, B.S. haran, A. Durairajan, R.E. White, Y. Podrazhansky, B.N. Popove, *J. Power Sources* 91 (2000) 122–129.
- [8] F. Huet, *J. Power Sources* 70 (1998) 59–69.
- [9] S. Rodrigues, N. Munichandraiah, A.K. Shukla, *J. Solid State Electrochem.* 3 (1999) 397–405.
- [10] Y. Podrazhansky, R. Cope, in: *Proceedings of the Meeting Abstracts of 198th Electrochemical Society Meeting, Phoenix, Arizona, 22–27 October 2000*, p. 59.
- [11] G. Nagasubramanian, *J. Power Sources* 87 (2000) 226–229.
- [12] B.A. Boukamp, *Equivalent Circuit, Users Manual*, University of Twente, The Netherlands, 1989.
- [13] F.C. Laman, M.W. Matsen, J.A.R. Stiles, *J. Electrochem. Soc.* 133 (1986) 2441.
- [14] N.A. Hampson, S.A.G.R. Karunathilaka, R. Leek, *J. Appl. Electrochem.* 10 (1980) 3.
- [15] M.G.S.R. Thomas, P.G. Bruce, J.B. Goodenough, *J. Electrochem. Soc.* 132 (1985) 1521.
- [16] M. Yoshio, H. Tanaka, K. Tominaga, H. Noguchi, *J. Power Sources* 40 (1992) 347–353.
- [17] Ech-Duck Jeong, Mi-Sook Won, Yoon-Bo Shim, *J. Power Sources* 70 (1998) 70–77.
- [18] H. Wang, Y.-I. Jang, B. Huang, D.R. Sadoway, Y.-M. Chiang, *J. Electrochem. Soc.* 146 (1999) 473.
- [19] G.G. Amatucci, J.M. Tarascon, L.C. Klein, *Solid State Ion.* 83 (1996) 167.
- [20] D. Aurbach, B. Markovsky, I. Weissman, E. levi, Y. Ein-Eli, *Electrochim. Acta* 45 (1999) 67–86.
- [21] J.-S. Kim, Y.-T. Park, *J. Power Sources* 91 (2000) 172–176.
- [22] A.M. Andersson, K. Edstrom, N. Rao, A. Wendsjo, *J. Power Sources* 81/82 (1999) 286–290.
- [23] Y. Matsumura, S. Wang, J. Mondori, *J. Electrochem. Soc.* 142 (1995) 2914.
- [24] Pankaj Arora, Ralph E. White, *J. Electrochem. Soc.* 145 (1998) 3647.